

# Lamellar Liquid Single Crystal Hydrogels: Synthesis and Investigation of Anisotropic Water Diffusion and Swelling

Felix Kleinschmidt,<sup>†</sup> Markus Hickl,<sup>†</sup> Kay Saalwächter,<sup>†</sup> Claudia Schmidt,<sup>\*,‡</sup> and Heino Finkelmann<sup>\*,†</sup>

*Institut für Makromolekulare Chemie, Universität Freiburg, Stefan-Meier-Str. 31, D-79104 Freiburg, Germany, and Department Chemie, Universität Paderborn, Warburger Strasse 100, D-33098 Paderborn, Germany*

Received July 7, 2005

**ABSTRACT:** The synthesis and characterization of anisotropic liquid single crystal hydrogels (LSCHs) via photoinduced radical polymerization of magnetically aligned samples in the lyotropic mesophase are reported, which are stable against tensile stresses in all three dimensions. The hydrogels exhibit a lamellar phase ( $L_a$ ) in the swollen state. The high mechanical stability is achieved by using a new type of cross-linker. Monomer and cross-linker molecules have almost the same chemical constitution, varying only in the number of polymerizable groups. The cross-linker is incorporated perfectly into the liquid-crystalline phase structure of the lyotropic liquid-crystalline monomers, yielding a network which has covalent bridges between the lamellae. The anisotropic hydrogels are characterized by a variety of methods on micro- and macroscopic length scales. Swelling with the nonselective solvent toluene shows that cross-linking within the liquid-crystalline phase causes an anisotropic topology of the network, which shows a memory effect even in the isotropic phase. Time- and temperature-dependent pulsed field gradient diffusion NMR measurements yield a ratio of the order of 10:1 for the self-diffusion coefficients of  $D_2O$  perpendicular and parallel to the layer normal. A step in the diffusivity across the lamellae at 312–314 K is interpreted by a disruption of the lamellae caused by elastic forces due to anisotropic network deformation as a function of temperature or by an increased porosity of the membranes in analogy to a lamellar-to-sponge transformation. Hygroelastic measurements, in which the length and width of the hydrogels are measured as a function of their controlled water sorption, show an anisotropic swelling behavior consistent with the structure of a lamellar phase. The isotropic-to-lamellar phase transformation upon increasing water concentration leads to a flattening of the polymer coil along the layer normal. Swelling with water in the lamellar phase is anisotropic.

## I. Introduction

Macroscopic anisotropy, leading for example to birefringence and anisotropic swelling, is a remarkable property of lyotropic liquid single crystalline hydrogels (LSCHs). LSCHs are water-swollen cross-linked amphiphilic polymers forming spontaneously a macroscopically aligned lyotropic liquid crystal phase. In LSCHs the properties of different classes of materials are combined. On one hand, LSCHs show the typical behavior of elastomers such as form stability and rubber elasticity, and on the other hand, they feature the properties of liquid crystals such as self-organization and physical anisotropy. Such liquid-crystalline elastomers on the basis of lyotropic liquid crystals are of particular interest because they allow a comparison with the corresponding thermotropic liquid-crystalline elastomers which have been an object of research for two decades.<sup>1,2</sup> In particular, questions regarding the network topology in the two types of liquid-crystalline networks are not answered yet. Besides this important academic question, LSCHs are also expected to have interesting applications. A prototype of a bifocal contact lens making use of the birefringence which causes two indices of refraction has already been developed.<sup>3</sup> LSCH systems are also discussed as models of artificial cell membranes.<sup>4</sup>

Several methods to obtain LSCHs were recently reported.<sup>3,5–8</sup> The first approach by Löffler proved that cross-linked polyamphiphiles indeed exhibit lyotropic liquid-crystalline phases when swollen with water.<sup>7</sup> The mechanical stress caused by the uniaxial swelling of a lyotropic hexagonal phase in a glass tube led to a macroscopic alignment of the liquid crystal. Fischer succeeded in obtaining the first liquid-crystalline hydrogel with permanent uniform orientation of the director of the liquid-crystalline phase.<sup>5</sup> Those hydrogels were realized in a two-step reaction. In the first step, a conventional nonionic surfactant is polymerized, and the polymer is weakly cross-linked in the same batch. In the second step, a mechanical stress is applied, which forces the polymeric chain into a nonspherical conformation, and the cross-linking process is completed under strain. The deformation of the macromolecules fixed in this way causes an orientation of the micelles when a lyotropic phase is formed by water absorption. For systems forming a lamellar phase, uniaxial extension of the elastomer results in an alignment of the layer normal vectors (directors) perpendicular to the axis of extension, whereas uniaxial compression leads to a lamellar monodomain with the director parallel to the axis of compression.<sup>5,6</sup> Fischer also reported first results on the hygroelastic effect, that is, the anisotropic macroscopic swelling of a substance upon water sorption, which is caused by elastic stresses due to the coupling between the network and the liquid crystalline order.<sup>5</sup>

A different approach toward oriented hydrogels was taken by Amigó-Melchior.<sup>3</sup> On the basis of the knowl-

<sup>†</sup> Universität Freiburg.

<sup>‡</sup> Universität Paderborn.

\* Corresponding authors. E-mail: Claudia.Schmidt@uni-paderborn.de; Heino.Finkelmann@makro.uni-freiburg.de.

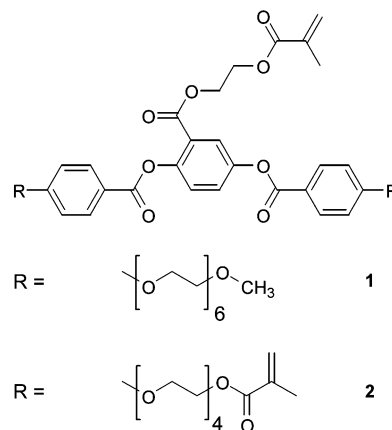
edge that rigid anisometric surfactant molecules<sup>9–13</sup> lead to the formation of micelles with a specific geometry<sup>14</sup> due to packing restraints, a polymerizable amphiphile was developed. The molecule had to form a lyotropic liquid-crystalline phase, preferably a lamellar one ( $L_\alpha$ ), over a broad temperature and concentration range. Additionally, a high anisotropy of the diamagnetic susceptibility was needed. This should allow for the uniform orientation of the liquid-crystalline phase structure by a magnetic field in order to form a monodomain before polymerization. The desired molecule was found by subsequent alteration of the spacer length and the hydrophilic/hydrophobic balance (HLB)<sup>3,15</sup> of a rodlike amphiphile with an aromatic core.<sup>16</sup> The rodlike shape causes a lamellar structure, and the aromatic rings lead to the positive diamagnetic anisotropy that is required for a uniform layer orientation in a magnetic field. For the first hydrogels based on this monomer a hydrophobic cross-linker molecule was used. In this system the density of cross-linking within the hydrophobic part of the smectic layers was higher than the density of interlayer cross-linking, which caused a lack of mechanical stability. Similar effects are known from thermotropic liquid-crystalline elastomers, where the type of cross-linking influences the mechanical behavior. Interlayer and intralayer cross-linking result in different moduli of elasticity.<sup>17–19</sup> It was also shown that the coupling between liquid-crystalline phase and polymer network differs.<sup>20,21</sup>

In the present work we follow the approach of Amigó-Melchior but introduce a new type of cross-linker molecule, which is adapted to the amphiphilic structure of the monomer and can therefore be incorporated perfectly into the lamellar phase. This cross-linker has polymerizable groups in both its hydrophilic and hydrophobic parts. Therefore, cross-linking should occur not only within the layers but also between adjacent layers, and a three-dimensionally stable network is expected. The polymerization and the cross-linking process are carried out in one step in the magnetically aligned aqueous liquid-crystalline phase.

Important questions concern the microscopic properties of these new hydrogels, such as membrane ordering and permeability, and the macroscopic anisotropy and order of the material on different length scales. The investigation of its anisotropic swelling with water should provide information about the influence of the phase transformation on the chain conformation of the polymer. We were particularly interested in how this new type of cross-linking influences the topology of the network and whether this network, which was formed in the liquid-crystalline phase, differs from earlier ones that were cross-linked in isotropic solution in a nonselective solvent.

To answer these questions, we carried out complementary physical measurements on different length scales in order to obtain a picture as complete as possible of the properties of these new materials. The hydrogels were characterized on a macroscopic level with optical microscopy, stress–strain, swelling, and hygroelastic measurements and on a micro- and mesoscopic scale by X-ray diffraction, deuterium NMR spectroscopy, and diffusion measurements. In the following, after the Experimental Section, we will show that our synthetic concept yields mechanically stable LSCHs. In section IV, the results of pulsed field gradient diffusion experiments will be presented that not only confirm the

### Scheme 1. Structure of the Amphiphilic Monomer and Cross-Linker



anisotropy of the hydrogels and establish differences arising from different preparation conditions but also show an unexpected temperature dependence of diffusion. In section V the results of the hygroelastic measurements are discussed which reflect the chain conformation. Section VI summarizes the major conclusions.

## II. Experimental Section

**Synthesis.** All reactions were carried out in an argon atmosphere to prevent oxidation of the ethylene glycols. The reactions with molecules containing methacrylic groups were carried out in darkness by using glass apparatuses wrapped in aluminum foil to prevent spontaneous polymerization.

*Synthesis of the Monomer and the Cross-Linker.* The lyotropic hydrogels were synthesized from the amphiphilic monomer **1** and the adapted cross-linker molecule **2** shown in Scheme 1. The monomer has a side-on methacrylate function that can undergo radical polymerization in aqueous solution. Its lyotropic phase behavior and that of its homopolymer have already been investigated;<sup>3</sup> the binary phase diagrams are shown in Figure 1. The cross-linker molecule is a modification of the monomer and has almost the same chemical structure. It has three methacrylate groups: one attached side-on to the hydrophobic part as for the monomer and the other two attached end-on to the hydrophilic moieties.

*2,5-Di-(4-{2-[2-(2-{2-(2-Methoxyethoxy)ethoxy}ethoxy)ethoxy]ethoxy}benzoic acid ester)benzoic acid 2-(2-methylacryloyloxy)ethyl ester (1)* was prepared by using the same procedures as described by Amigó-Melchior.<sup>3</sup> The purification of **1** was improved by using column chromatography with Sephadex LH 20, a modified dextran gel liquid chromatography medium, as stationary phase and methanol as mobile phase. To prevent spontaneous polymerization, the substance was stored in cryo tubes using liquid nitrogen as cooling medium.

The route for the synthesis of the cross-linker is presented in Scheme 2. It starts with the preparation of the hydrophilic tails of the molecule. The complete cross-linker is gained in the very last step by connecting the tails **8** with the core molecule **3**. In this step the rigid hydrophobic part is formed. The sequence begins with the protection of one of the two alcoholic functions of tetraethylene glycol. This step is followed by the esterification of the glycol with *p*-hydroxybenzoic acid methyl ester using the Mitsunobu procedure.<sup>22</sup> In the next two steps the protection groups of the glycol **4** and benzoic acid are removed using standard procedures. The polymerizable group is introduced by an azeotropic esterification of the deprotected alcoholic function of glycolbenzoic acid (**7**) with methacrylic acid. In the final step the side parts **8** and the core of the molecule **3** are connected via an esterification with *N,N'*-dicyclohexylcarbodiimide.

*2-(2-{2-[2-(2-(2-Tetrahydropyran-2-yloxy)ethoxy}ethoxy)ethoxy]ethoxy)ethanol (4)* was obtained by a monoprotection of tetraethylene

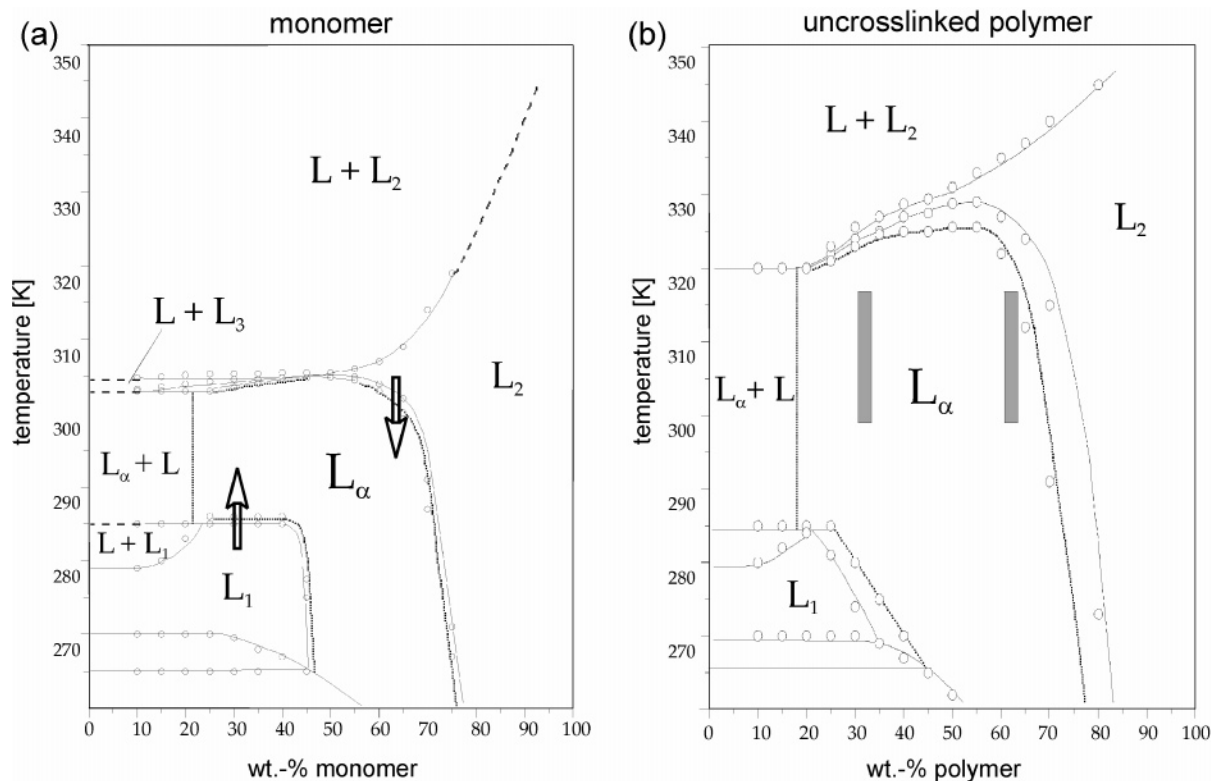
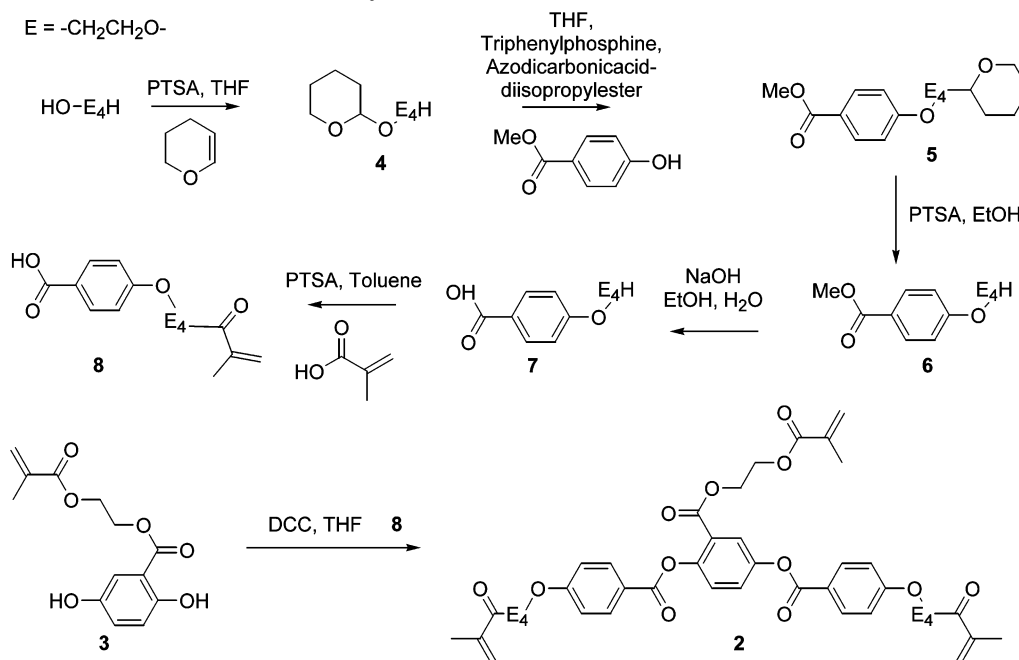


**Figure 1.** Phase diagram of the monomer **1** (left) and the corresponding un-cross-linked polymer (right) in  $D_2O$ .<sup>3</sup> The arrows in (a) indicate the temperature pathway during the alignment procedure in the magnetic field. The gray bars in (b) show the regions where diffusion was measured.

### Scheme 2. Synthesis of the Cross-Linker Molecule



glycol with a tetrahydropyran group. 116.5 g (0.6 mol) tetraethylene glycol and 10 g of *p*-toluenesulfonic acid (PTSA) were dissolved in 200 mL of tetrahydrofuran (THF). 25.2 g (0.3 mol) of dihydropyran were added dropwise. The mixture was stirred at room temperature for 2 h to form **4**. THF was removed by distillation. The crude product was dissolved in chloroform and washed with water. After drying with  $MgSO_4$  and removal of the solvent, the product was used without further purification [yield: 50 g of a clear liquid containing 70% monoprotected and 30% diprotected glycol according to gas chromatography].

4-[2-(2-{2-[2-(Tetrahydropyran-2-yloxy)ethoxy]ethoxy}ethoxy)ethoxy]benzoic acid methyl ester (**5**) was prepared by esterifi-

cation of **4** with *p*-hydroxybenzoic acid methyl ester using the Mitsunobu procedure. 50 g of the monoprotected glycol (0.125 mol contained in the mixture described above), 16.2 g (0.125 mol) of *p*-hydroxybenzoic acid methyl ester, and 33 g of triphenylphosphine were dissolved in 300 mL of THF. 25.5 g (0.125 mol) of azodicarbonic acid diisopropyl ester was added dropwise. The mixture was stirred overnight. After removal of the solvent diethyl ether was added, and a colorless precipitate of byproducts was formed. It was filtered off, and the ether was removed by distillation.

4-(2-[2-(2-Hydroxyethoxy)ethoxy]ethoxy)benzoic acid methyl ester (**6**) results after deprotection of the glycol. The

crude product of the preceding reaction was dissolved in ethanol. 3 g of pyridinium *p*-toluenesulfonic acid was added. The pH of the solution was 3. The mixture was refluxed for 3 h, and then the ethanol was removed in a vacuum. The crude product was dissolved in chloroform and washed with water. After drying with MgSO<sub>4</sub> and removal of the solvent, the product was used in the next step without further purification.

4-(2-[2-[2-(2-Hydroxyethoxy)ethoxy]ethoxy]ethoxy)benzoic acid (**7**) was obtained by deprotection of the carbonic acid. The crude product of the preceding reaction was dissolved in 600 mL of a water/methanol mixture (2:1). 10 g (0.41 mol) of lithium hydroxide was added. The mixture was refluxed for 3 h. The methanol was removed by vacuum distillation. Hydrochloric acid was added, and the product was extracted with chloroform. The solution was dried with MgSO<sub>4</sub> and the chloroform removed. The product was purified by multiple recrystallization from ethyl acetate/cyclohexane (1:1) [yield: 10 g of a colorless wax, 25% with respect to **4** after three reaction steps].

<sup>1</sup>H NMR (300 MHz, CDCl<sub>3</sub>): δ [ppm] = 3.7 (t, 3 H, CH<sub>2</sub>-CH<sub>2</sub>-OH), 3.8 (m, 10 H, glycol), 4.0 (t, 2 H, COO-CH<sub>2</sub>-CH<sub>2</sub>), 4.2 (t, 2 H, COO-CH<sub>2</sub>), 7.0 (d, 2 H, Ar-H), 8.1 (d, 2 H, Ar-H).

4-[2-(2-[2-(2-Methylacryloyloxy)ethoxy]ethoxy]ethoxy)ethoxy]benzoic acid (**8**) was prepared by functionalization of **7** with methacrylic acid. A mixture of 7.5 g (0.024 mol) of **7**, 10 g (0.12 mol) of methacrylic acid, and 0.2 g of *p*-toluenesulfonic acid in chloroform was refluxed in a Dean-Stark apparatus for 72 h. The chloroform and the excess methacrylic acid were removed by vacuum distillation. The crude product was purified by column chromatography (silica gel F60, ethyl acetate) [yield: 6.3 g (68%) of a colorless wax].

<sup>1</sup>H NMR (300 MHz, CDCl<sub>3</sub>): δ [ppm] = 1.9 (s, 3 H, CH<sub>2</sub>=C(CH<sub>3</sub>)-COO), 3.6 (m, 10 H, glycol), 3.9 (t, 2 H, COO-CH<sub>2</sub>-CH<sub>2</sub>), 4.2 (t, 2 H, COO-CH<sub>2</sub>), 4.3 (t, 3 H, CH<sub>2</sub>-CH<sub>2</sub>-OOC-C(CH<sub>3</sub>=CH<sub>2</sub>), 5.5 (s, 1 H, CH<sub>2</sub>=C(CH<sub>3</sub>)-COO), 6.1 (s, 1 H, CH<sub>2</sub>=C(CH<sub>3</sub>)-COO), 6.9 (d, 2 H, Ar-H), 8.0 (d, 2 H, Ar-H).

2,5-Dihydroxybenzoic acid 2-(2-methyl-acryloyloxy)ethyl ester (**3**) was prepared using the procedure described by Amigó-Melchior.<sup>3</sup>

2,5-Di-(4-[2-(2-[2-(2-Methylacryloyloxy)ethoxy]ethoxy)ethoxy]ethoxy)benzoic acid ester)benzoic acid 2-(2-methyl-acryloyloxy)ethyl ester (**2**) was obtained by linking **8** and **3**. All substances were vacuum-dried. 2.5 g (0.0065 mol) of **8**, 0.9 g (0.0033 mol) of **3**, and 80 mg of *p*-(dimethylamino)pyridine were dissolved in dry methylene chloride. The mixture was cooled in an ice bath. 1.3 g (0.0065 mol) of *N,N'*-dicyclohexylcarbodiimide (DCC) was added. The mixture was allowed to warm to room temperature and stirred for 3 h. The precipitate which was formed during the reaction was filtered off. The solution was washed with HCl solution and sodium bicarbonate solution consecutively. The solution was dried with MgSO<sub>4</sub> and the solvent removed by distillation. The cross-linker was purified by column chromatography (Sephadex LH 20, methanol). To prevent spontaneous polymerization, the substance was stored in cryo-tubes using liquid nitrogen as cooling medium [yield: 1 g (30%) of a colorless, viscous liquid].

<sup>1</sup>H NMR (300 MHz, CDCl<sub>3</sub>): δ [ppm] = 2.1 (s, 9 H, CH<sub>2</sub>=C(CH<sub>3</sub>)-COO), 3.9 (m, 20 H, glycol), 4.1 (t, 4 H, Ar-O-CH<sub>2</sub>-CH<sub>2</sub>), 4.35 (m, 6 H, Ar-COO-CH<sub>2</sub>-CH<sub>2</sub> and Ar-O-CH<sub>2</sub>-CH<sub>2</sub>), 4.5 (t, 4 H, CH<sub>2</sub>=C(CH<sub>3</sub>)-COO-CH<sub>2</sub>-glycol), 4.6 (t, 2 H, CH<sub>2</sub>=C(CH<sub>3</sub>)-COO-CH<sub>2</sub>-CH<sub>2</sub>-OOC-Ar), 5.7 (s, 3 H, CH<sub>2</sub>=C(CH<sub>3</sub>)-COO), 6.3 (s, 3 H, CH<sub>2</sub>=C(CH<sub>3</sub>)-COO), 7.1 (dd, 2 H, Ar-H), 7.4 (d, 1 H, Ar-H), 7.6 (dd, 1 H, Ar-H), 8.05 (d, 1 H, Ar-H), 8.3 (d, 2 H, Ar-H).

**Synthesis of LSCH Samples.** To produce the hydrogels monomer, cross-linker, deuterium oxide, and photoinitiator (Ciba Irgacure 2959 and Ciba Darocure 1173 1:1) were mixed in a Teflon capsule using a Perkin-Elmer vibrating mill. Two different types of samples were prepared. For the NMR measurements the thoroughly homogenized mixture was filled through a capillary of 0.5 mm inner diameter into a small sphere (4 mm diameter) of quartz glass. The sample was then sealed by melting of the capillary. For all other investigations the mixture was filled in a Teflon mold of a stripe form (20 mm × 5 mm × 0.4 mm), covered by a quartz glass plate. Both

types of samples were aligned in an NMR magnet (11 T for the spherical samples and 7 T for the stripes) to obtain a uniform director orientation. For the stripes of length *z* and width *x* the layer normal (director) is parallel to *z*. The lamellar phase (L<sub>α</sub>) was reached by slowly heating or cooling from the isotropic phases (L<sub>1</sub> or L<sub>2</sub>, cf. Figure 1) and subsequent annealing in the biphasic region. The process of orientation was followed by <sup>2</sup>H NMR. At the starting temperature a narrow single peak is observed in the isotropic phase. In the two-phase region the quadrupolar doublet grows at the expense of the central isotropic peak. The lamellar phase shows a pure doublet of narrow lines. Within the highly viscous mesophase, the orientation of the molecules is stable, and the sample can be removed from the magnetic field for the polymerization, which was carried out in a Kulzer Dentacolor XS UV lamp equipped with two xenon lamps. The irradiation wavelength was 320–520 nm. The exposure time was 120 s. A home-built cooling device which uses a liquid nitrogen cooled gas stream allows us to control the temperature within the polymerization chamber of the UV-lamp. The temperature was kept at 293 K during the polymerization process.

The stripe-shaped hydrogels were stored in the swollen state in bidistilled water. The stripes are stable against slight mechanical deformation in all directions of space. The water can be removed from the stripes without damaging them. If they are penetrated with water again, they regain their initial appearance. The dry elastomers exhibit common rubber elasticity.

**Measurements. X-ray Measurements.** The hydrogel samples were placed in water in a 2 mm diameter glass capillary. Diffraction studies were performed with a rotating anode generator (6.4 kW) in a point-collimated Kiessig camera with Ni-filtered Cu Kα radiation (wavelength λ = 1.542 Å) at a distance of 180 mm. Two-dimensional patterns were recorded with an image plate system (Schneider, Freiburg).

**NMR Measurements.** <sup>2</sup>H NMR spectra were recorded on a Bruker Avance 500 spectrometer (11.7 T) at a frequency of 76.773 MHz. Orientation-dependent measurements were performed using a goniometer probe with a 5 mm solenoid coil. The sample can be rotated about an axis perpendicular to the external magnetic field. Orientation of the monodomains used for hydroelastic measurements were performed on a Bruker MSL spectrometer (7 T), operating at a frequency of 46.073 MHz. The polymerization mold was placed in a 15 mm saddle coil. The sample temperature was kept constant within 1 K by a Eurotherm thermostat.

**Pulsed Gradient Diffusion NMR.** Pulsed-field gradient measurements of the self-diffusion coefficient *D* were performed in a Bruker high-resolution probe with a singly tuned saddle coil (~5 μs 90° pulses) using the pulsed gradient stimulated-echo technique (PGSTE). The standard method of Steijskal and Tanner<sup>23,24</sup> and its basic theory are extensively covered in the literature.<sup>25</sup> A matched pair of trapezoidal ramped gradient pulses, separated by the diffusion time Δ, was inserted in the evolution delays *t*<sub>2</sub> of the stimulated echo sequence 90°-*t*<sub>2</sub>-90°-*t*<sub>1</sub>-90°-*t*<sub>2</sub>-aq. The attenuation of the spin-echo intensity due to diffusion is given by

$$\ln\left(\frac{S}{S_0}\right) = -4\pi^2 q^2 D(\Delta - \delta/3) \quad (1)$$

where a correction for the finite duration of the gradient pulses, δ, is included. *S*<sub>0</sub> is the signal intensity with gradient amplitudes of zero. The "wave vector" *q* = γδ*g*/(2π) further depends on the magnetogyric ratio γ and the gradient amplitude *g*. During one diffusion experiment all delays are kept constant, and the gradient amplitude *g* is incremented. Gradients were calibrated to the known diffusion coefficient of D<sub>2</sub>O.<sup>26</sup> Diffusion parallel to the layer normal was measured with the Bruker Diff30 gradient system (which has a stronger gradient), whereas diffusion perpendicular was measured with the Bruker Micro5 imaging system with three orthogonal gradient coils.

**Table 1. Composition of the Polymerized Mixtures in wt %<sup>a</sup>**

sample name	HG33d	HG33h	HG65d	HG65h
amphiphile	28.5	32.2	59.3	64.1
cross-linker	1.9	2.6	3.0	3.7
cross-linker relative to pure amphiphile	6.3	7.5	4.8	5.8
D <sub>2</sub> O	68.6	64.2	36.7	31.2
photoinitiator	1.0	1.0	1.0	1.0

<sup>a</sup> The suffix of each hydrogel labels the type of experiment: *d* = diffusion; *h* = hygroelastic.

**Swelling Behavior and Hygroelastic Measurements.** The isotropic swelling with the nonselective solvent toluene was measured under a Will Strübin reflection microscope. The dimensions were measured before and after swelling, and the swelling coefficients  $\lambda_z$  in length and  $\lambda_x$  in width were calculated by dividing the length (*z*) or width (*x*) in the swollen state by the respective initial dimensions. Because of the uniaxiality of the system,  $\lambda_y$  was taken equal to  $\lambda_x$  and the swelling parameter *q*, defined as the volume ratio of the swollen and dry sample, was calculated according to

$$q = \lambda_z \lambda_x^2 \quad (2)$$

The macroscopic dimensions of the hydrogel as a function of the water concentration is measured with the method of hygroelasticity, which allows us to measure the change of dimensions of hydrogels during the process of swelling by controlling precisely the content of water in the sample. The measurements are carried out in a home-built computer-controlled apparatus, equipped with a hygostat. This hygostat operates by the isopiestic principle. At a given temperature  $T_2$  the sample is equilibrated with the partial pressure of water,  $p_{H_2O}$ . This partial pressure can be altered if nitrogen gas is saturated with water at a temperature  $T_1$ , where  $T_1 < T_2$ . Water is absorbed by the hydrogel depending on  $p_{H_2O}$ . The resulting change of the polymer concentration in the sample can be measured in situ with a microbalance (Sartorius MP4040). The relative dimensions of the sample are quantified via a CCD camera.

### III. Results and Discussion

**Preparation and Characterization of Lamellar LSCHs.** On the basis of the known phase diagram of the monomer/D<sub>2</sub>O system,<sup>3</sup> depicted in Figure 1, several hydrogels were prepared at concentrations at which the aqueous solutions can be aligned in a magnetic field by cooling or heating slowly from an isotropic phase into the lamellar phase as indicated by the arrows in Figure 1. Because of the positive anisotropy of the diamagnetic susceptibility of the aromatic molecules, this procedure leads to an alignment of the long axes of the molecules parallel to the magnetic field, resulting in macroscopically aligned lamellar samples. The mixtures which were used to produce the hydrogels are given in Table 1. Different concentrations of the amphiphile were chosen in order to investigate the influence of the initial structure of the lamellar phase on the properties of the LSCH resulting after polymerization and cross-linking. HG33d and HG33h were synthesized in the water-rich concentration range, whereas HG65d and HG65h were synthesized with a high concentration of amphiphile. They were found to be macroscopically aligned lamellar systems as will be shown in the following.

The dry isotropic hydrogels prepared with the new cross-linker that enables intra- and interlamellar cross-linking are mechanically stable against tensile stress in all directions. A stress-strain experiment of elastomer HG33h showed a linear relationship between the stress and the strain  $z/z_0$  up to a strain of 1.5. A Young

**Table 2. Relative Changes of the Lengths ( $\lambda_z$ ) and Widths ( $\lambda_x$ ) of the Hydrogels in the Isotropic State Swollen with the Nonselective Solvent Toluene**

sample	$\lambda_z$	$\lambda_x$
HG33h	1.64	1.76
HG65h	1.61	1.74

modulus of 24 kPa was determined. This value is comparable with the Young modulus of a smectic elastomer in the isotropic phase.<sup>27</sup>

When studying the macroscopic anisotropy of the material, the important question arises if the cross-linking process within the liquid crystalline phase influences the topology of the network. This can be tested by swelling measurements in the isotropic phase, using a nonselective solvent that does not induce the formation of micellar aggregates and lyotropic mesophases. An anisotropy of swelling under these conditions indicates an intrinsic anisotropy of the network due to the conditions under which the cross-linking process occurred. In Table 2 the results of swelling experiments with the nonselective solvent toluene are summarized.

Actually both samples exhibit anisotropic swelling by the nonselective solvent. The relative change in the dimension  $\lambda_x$  is larger than  $\lambda_z$ . This means that the polymerization and cross-linking process which occurred in the liquid-crystalline phase yields a degree of cross-linking that is higher for interlayer cross-linking than for intralayer cross-linking. In other words, the network strands parallel to the layer normal are shorter than those perpendicular to it. This is plausible when the molecular structure of the cross-linker molecule is considered. The cross-linker is hexafunctional since two network chains start from each methacrylate group. Only two of the six functions are located in the hydrophobic regions, where most of the methacrylate groups of the monomers are, but four are in the hydrophilic region. Because of this structure, it is most likely that the functional groups of the cross-linker in the hydrophilic regions react with each other (or with the hydrophilic ethylene oxide chains in their neighborhood), resulting in very short strands, whereas all functional groups in the hydrophobic part can react with each other, leading to longer chains between branching points. This structural model is supported by the earlier results obtained by Amigo-Melchior.<sup>3</sup> He observed poor mechanical stability due to a lack of interlayer cross-links for hydrogels synthesized with a cross-linker that had no hydrophilic moieties with functional groups. The swelling of the dry hydrogels proves that the deswollen gel remembers the topology of the network formed in the liquid-crystalline phase; the networks prepared in the liquid crystalline phase have an intrinsic anisotropy.

The optical quality of the hydrogels, which are transparent, was investigated by polarization microscopy. The gels were studied in the swollen state between crossed polarizers. If the polarization axis is parallel to the optical axis of the hydrogel, complete extinction of the light is expected. However, we obtained the photograph shown in Figure 2 (left). The picture with an orientation of the director of the liquid-crystalline phase parallel to the axis of polarization shows a characteristic defect structure, known as focal conics, instead of complete extinction of the light. The focal conic structure was proposed by Friedel and Grandjean.<sup>28</sup> In these defects the layers take the form of uniformly spaced Dupin cyclides. A cross section through a set of Dupin cyclides as they appear in a focal conic structure is

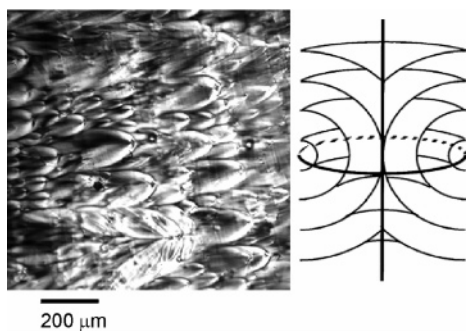


**Figure 2.** Optical microscopy picture of the swollen hydrogel between crossed polarizers with the orientation of the director parallel to the axis of polarization (left) and cross-section through a set of Dupin cyclides as they appear in the focal conic texture (right).

drawn in Figure 2 (right). These defects are well-known from smectic liquid crystals<sup>29</sup> but have also been found in lyotropic liquid crystals containing surfactants.<sup>30,31</sup> The process by which these arrays form is not entirely clear. It is known that the planar regions which develop between the oily streaks during the annealing process ultimately transform into focal conic arrays. Interestingly, the orientations of the defects are not distributed randomly over the sample, which would indicate a polydomain. They form perfectly aligned arrays with the apex of the hyperbola showing in one direction. Furthermore, the apices are found on more or less straight lines. This indicates that the lamellar hydrogel is macroscopically aligned but not free of defects.

The proof of the macroscopic alignment of the sample is provided by two-dimensional X-ray diffraction using an image plate geometry. The swollen hydrogel at 295 K exhibited a diffraction pattern with one sharp single-point Bragg reflection in the small-angle region, characteristic of an aligned lamellar phase. The lamellar period is 63 Å. For comparison, the monomer in its all-trans conformation has a length of 65 Å. The analysis of the azimuthal width of the Bragg peaks according to the model of Mitchell<sup>32,33</sup> yields a domain order parameter  $S_{X\text{-ray}} = 0.65$ . Assuming an exponential loss of interlayer correlation, the peak shape as a function of the polar scattering angle can be fitted with a Lorentzian function. From the inverse of its full width at half-maximum,<sup>34</sup> a smectic correlation length  $\xi_s$  is obtained as  $420 \pm 8$  Å, which corresponds to 6.7 layers.

The existence of a macroscopically oriented lamellar phase is confirmed by angular dependent <sup>2</sup>H NMR spectroscopy. The quadrupolar splitting of a uniaxial phase is related to the angle  $\beta$  between director and magnetic field by

$$\Delta\nu \propto \frac{1}{2}(3 \cos^2 \beta - 1) \quad (3)$$

If the system has a uniformly aligned lamellar phase, the quadrupolar splitting of a sample whose director is perpendicular to the magnetic field is exactly half of the quadrupolar splitting of a sample whose director is parallel to the magnetic field. The splitting vanishes at the magic angle of 54.7°. The observed splitting  $\Delta\nu$  of the hydrogels (830 Hz for HG65d and 720 Hz for HG33d at 303 K) as a function of the sample orientation follows perfectly a Legendre polynomial of second order, as given by eq 3. This proves that the lamellar structure of the monomer mixture is maintained during the process of polymerization.

The orientation-dependent NMR spectra yield also information on the degree of orientational order. The width and symmetry of the deuterium line shape depend on the natural line width (due to relaxation) and on the orientational distribution function of the local director. The estimation of the orientational distribution from NMR line shapes is a typical ill-posed inverse problem. A Tikhonov regularization procedure employing a self-consistent method to find the regularization parameter has proven particularly reliable in finding the solutions to such problems.<sup>35,36</sup> We used the procedure developed by Winterhalter et al.<sup>37</sup> to obtain the orientational distribution function of the director by Tikhonov regularization from two NMR signals, recorded at different angles  $\beta$  of the symmetry axis of the sample with respect to the static magnetic field. The orientational distribution function found in this way has one peak with a maximum at an angle of zero. Its width and shape vary somewhat depending on the values of  $\beta$  chosen for the two NMR signals, probably due to angular dependent transverse relaxation times. Averaging the results of the orientational distribution functions obtained for different sets of data yields a value for the full width at half-maximum of 13.5°. Calculating a domain order parameter from the orientational distribution function according to Mitchell results in  $S_{\text{NMR}} = 0.89$ . This value is significantly larger than the value of  $S_{X\text{-ray}}$ . The difference is attributed to the diffusion of the water molecules, whereby the NMR spectrum represents a dynamic average over regions of the sample spanning several micrometers. Disorder on an even smaller length scale, which is detected by X-ray scattering, is not detected in the NMR experiment.

The different techniques of characterization show that the synthetic concept has been successful for the preparation of mechanically stable lamellar hydrogels with a macroscopically uniform director orientation. Further information about the phase structure is provided by the investigation of the diffusion of water as described in the following section.

**Diffusion Measurements.** Diffusion was measured for each composition in the direction parallel to the director (layer normal) and perpendicular to it, resulting in self-diffusion coefficients  $D_{\parallel}$  and  $D_{\perp}$ , respectively. The echo decays due to diffusion gained from the pulsed gradient experiments of HG65d and HG33d are presented in Figure 3 for varying diffusion times  $\Delta$  between 30 and 200 ms.

The linear dependence of the natural logarithm of the normalized echo amplitude  $S/S_0$  on the square of the parameter  $q$  (cf. eq 1) signifies that the echo decay has a Gaussian shape, which means that there are no restrictions to diffusion on the time scale of the experimental diffusion times  $\Delta$ . The diffusion time  $\Delta$  was varied from experiment to experiment while the gradient duration  $\delta$  and the maximum gradient amplitude  $g_{\text{max}}$  were chosen adequately to reach an echo intensity close to zero at  $g_{\text{max}}$ . Since all gradient parameters in the pulse sequence were varied independently, technical artifacts can be excluded. The diffusion coefficients were derived by fitting the raw data according to eq 1. No tendential dependence on  $\Delta$  was observed for any temperature, but the scattering of the data is bigger than their individual fitting error. Therefore, the mean value of the diffusion coefficients  $D_{\text{mean}}$  was taken, and the error interval was calculated from the different measurements with varying  $\Delta$ .

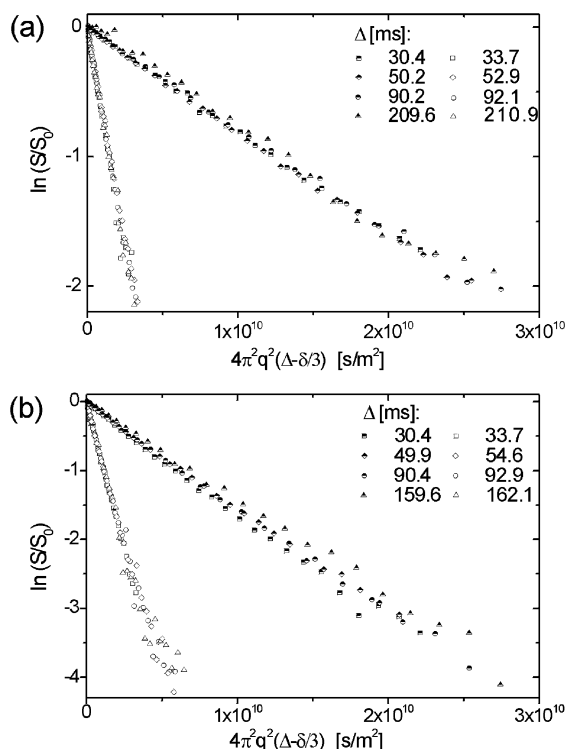


**Figure 3.** Diffusion time dependent spin-echo decay for HG65d and HG33d at 298 K. Half-filled and open symbols correspond to diffusion parallel and perpendicular to the layer normal, respectively.

**Table 3. Diffusion Coefficients of D<sub>2</sub>O and Mobile Protons at 298 K, Parallel and Perpendicular to the Layer Normal**

sample name	$D_{\text{mean}}(\text{D}_2\text{O})$ [ $10^{-10}$ m <sup>2</sup> /s]		$D_{\text{mean}}(^1\text{H})$ [ $10^{-10}$ m <sup>2</sup> /s]	
	parallel	perpendicular	parallel	perpendicular
HG33d	$0.84 \pm 0.02$	$7.09 \pm 0.07$	$0.72 \pm 0.02$	$4.20 \pm 0.12$
HG65d	$0.40 \pm 0.01$	$5.35 \pm 0.04$	$0.27 \pm 0.01$	$3.61 \pm 0.05$

The average diffusion coefficients of D<sub>2</sub>O and the mobile protonated components are summarized in Table 3. The measured values of  $D_{\parallel}$  and  $D_{\perp}$  indicate that, on one hand, diffusion across the layers is possible and, on the other hand, that the motion along the layers is not free. The diffusivity along the layers is reduced by about 50% compared to free water, which can be explained by the strong interaction with the ethylene oxide chains. The anisotropy of D<sub>2</sub>O diffusion,  $D_{\perp}/D_{\parallel}$ , was in the range of 13 for HG65d and a bit lower for HG33d. This anisotropy is lower than for low molecular weight lyotropic systems, where anisotropies of 17 and more were found.<sup>38,39</sup> For a lamellar lyotropic mixture of 40 wt % C<sub>10</sub>E<sub>3</sub>/D<sub>2</sub>O we found anisotropies in the diffusivity of D<sub>2</sub>O of more than 100.<sup>40</sup> Probably, the structure of the lamellar phase of the hydrogel is less perfect than that of low molecular weight lamellar systems due to the restrictions of the amphiphiles tethered to the polymer network. Another origin of defective lamellae could be the energy transfer to the sample during UV cross-linking, which might heat the sample locally and disturb the mesophase.

From the diffusion time dependent data an estimation of the minimal lateral and longitudinal extension of a “perfectly” ordered domain can be made. The length scale over which information is accessible is given by the square root of the mean squared displacement  $\sqrt{\langle z^2 \rangle}$  and can be calculated according to  $\langle z^2 \rangle = 2D\Delta_{\text{max}}$ .

The upper limit for the length scale is restricted by  $\Delta_{\text{max}}$ , the maximal experimentally accessible diffusion time, which is limited to 200 ms due to relaxation. Residual mobile components (2.56 ppm, 30% of the total signal), whether originating from un-cross-linked mesogens or remaining photoinitiator is not clear to us, were measured in the proton spectrum of the hydrogels. Their particularly long  $T_1$  relaxation time expanded the diffusion time to 1 s, thereby giving access to even longer time scales. Proton diffusion coefficients were also obtained by fitting the echo intensity decay curves, but including a constant term in eq 1 to account for the immobile network. As for D<sub>2</sub>O no dependence on  $\Delta$  was observed. From the data in Table 3, a lower estimate of the size of a homogeneously ordered domain can be given as  $7.3 \mu\text{m} \times 26.9 \mu\text{m} \times 26.9 \mu\text{m}$  for HG65d and  $12.0 \mu\text{m} \times 29.0 \mu\text{m} \times 29.0 \mu\text{m}$  for HG33d, where the smaller values refer to the extension of the domains parallel to the layer normal. With a layer distance of 63 Å this means that homogeneity parallel to the layer normal is given over 1160 layers for HG65d and 1900 layers for HG33d. It should be emphasized that this does not mean that HG33d is ordered more perfectly; it just gives the lower limit of homogeneity. The difference in the calculated numbers is owed to the difference in the diffusion coefficients. A direct comparison of the diffusion coefficients gives additional information about the state of order in the two hydrogels. All diffusion coefficients of HG65d are smaller than the ones of HG33d, with a larger difference for  $D_{\parallel}$ . Although the differences are small, this indicates that HG65d has less defective membranes and is better ordered.

The temperature dependence of the diffusion coefficients is analyzed in terms of the obstruction factor  $Q = D_{\text{measured}}/D_{\text{free}}$ . Here,  $D_{\text{free}}$  is the diffusion coefficient of bulk water and  $D_{\text{measured}}$  is the coefficient of obstructed diffusion in the lamellar system. Hence,  $Q$  is expected to be less than one and smaller values of  $Q$  correspond to more strongly hindered diffusion. We calculated  $Q$  using the temperature-dependent D<sub>2</sub>O diffusion coefficients,  $D_{\text{free}}$ , measured by Mills.<sup>26</sup> The temperature-dependent obstruction factors  $Q_{\parallel}$  and  $Q_{\perp}$  for diffusion across and parallel to the lamellae are shown in Figure 4 for HG33d and HG65d. The values of  $Q$  for HG33d are higher, that is, diffusion is less obstructed, as expected for the gel with higher content of water.  $Q_{\parallel}$  of HG65d shows a step in the diffusivity at around 312 K, a similar step can be seen for HG33d at around 314 K. The hindrance of the water diffusion perpendicular to the layers is reduced above these temperatures. The temperature dependence of  $Q_{\perp}$  shows only a continuous increase with temperature, as shown in Figure 4b.

The steps in  $Q_{\parallel}$  at 312 K for HG65d and at 314 K for HG33d indicate a formation of defects in the lamellae. They are observed in a temperature range where the un-cross-linked polymer is still in the liquid crystalline phase, but where the corresponding low molecular weight monomer mixture is already phase separated. Two factors may contribute to the breaking up of the lamellae. One is an elastic force from the network. The network has a higher cross-linking density between neighboring lamellae as shown above by the swelling experiments with toluene. Because of this anisotropy of the network, thermal expansion or contraction (due to rubber elasticity) may be anisotropic. This can generate an internal stress that leads to the partial disruption of the mesophase above a certain threshold.

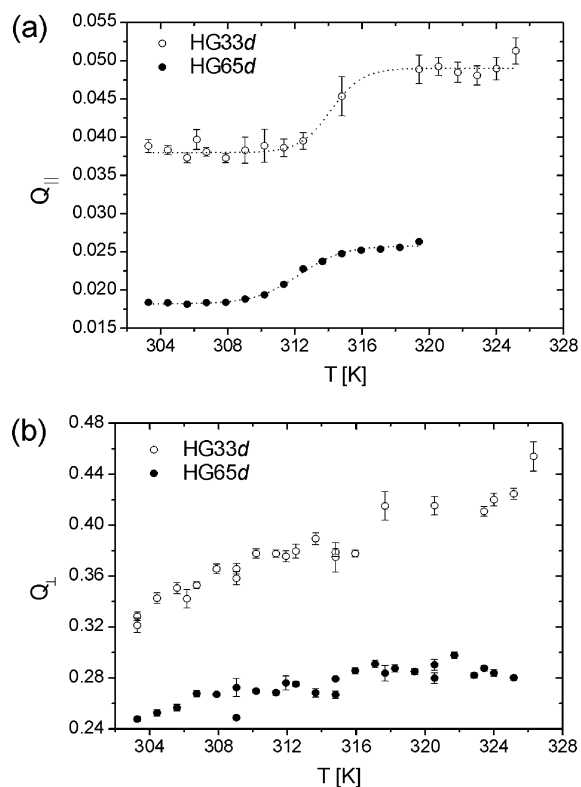


**Figure 4.** Results of the temperature-dependent PFG diffusion measurements given as  $D_2O$  obstruction factors  $Q_{\parallel}$  and  $Q_{\perp}$ . The dotted lines for  $Q_{\parallel}$  serve as a guide to the eye.

The other factor are the temperature-dependent properties of the amphiphile membranes. Similar to most oligo-(ethylene oxide) ether surfactants, the phase diagram of the monomer (cf. Figure 1) shows a sponge phase ( $L_3$ ) above the lamellar phase. This sponge phase results from the  $L_{\alpha}$  phase by partial fusion of adjacent membranes that lead to passages between the water layers and eventually to the bicontinuous structure of the  $L_3$  phase.<sup>41</sup> The  $L_3$  phase is isotropic and has a different topology than the  $L_{\alpha}$  phase, but on a local scale the membrane structure is preserved. It is conceivable that a similar transition in membrane topology occurs in the network (and also in the linear polymer) but that the structure above the transition remains anisotropic because the mobility of the amphiphiles is restricted by the polymer backbone. The creation of passages between neighboring water layers occurring at such a masked  $L_{\alpha}$ - $L_3$  transformation could explain the increased diffusivity perpendicular to the layers.

The anisotropy of diffusion on a macroscopic length scale can be visualized by the direct observation of the diffusion of a dye. Crystals of methylene blue and methyl red were put into the center of hydrogel HG33h at equilibrium degree of swelling. The diffusion of the dye was followed by taking pictures with a digital camera. An anisotropy of the diffusion is clearly visible in Figure 5a. By simply taking the squared ratio of the extensions of the stain perpendicular and parallel to the layers, an approximate  $D_{\perp}/D_{\parallel} = 5.3$  is obtained. An interpretation of this value in terms of diffusion anisotropy and large-scale defects is not straightforward, as it depends on the solubilities in the aqueous and organic parts of the sample. In this regard, the example of methyl red (Figure 5b) is particularly interesting, as it exhibits a reversed anisotropy. This more lipophilic dye appears to prefer crossing subsequent aqueous and

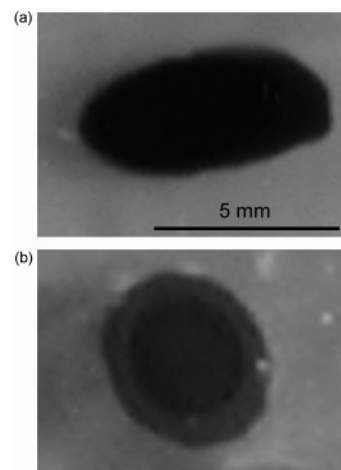


**Figure 5.** Macroscopic diffusion of (a) methylene blue and (b) methyl red, started from a crystal of the dye placed in the center of hydrogel HG33h, after 360 min. The layer normals are oriented vertically.

organic phases over diffusing along each of these, presumably because of the low mobility and small extension of the organic phase in which it preferably resides.

**Hygroelastic Measurements.** Detailed information about the topology of the network and the coupling between the liquid crystalline phase and the polymer network can be gained from swelling measurements. The preceding discussion of the swelling with a nonselective solvent has shown that the network has an intrinsic anisotropy. In the following, the influence on the phase transformation induced by swelling of the dried network with water, a solvent selective for the hydrophilic regions, is investigated. Therefore, we carried out hygroelastic experiments; that is, we measured the macroscopic changes of the dimensions of the hydrogels depending on their water content. These measurements allow us to draw conclusions on the microscopic structure of the hydrogels, in particular, on the conformations of the polymer chains and on the topology of the networks.

The main focus of this study concerns the influence of the micellar aggregation on the chain conformation of the polymer network. A macroscopically anisotropic behavior at the phase transformation and within the liquid-crystalline phase as shown schematically in Figure 6 is expected. The swelling factors of the length and width,  $\lambda_z$  and  $\lambda_x$ , have been calculated assuming constant partial molar volumes of water and network. Starting from the dry network with an isotropic polymer coil on the right-hand side of the diagram, the swelling in the isotropic  $L_2$  phase leads to a linear increase of  $\lambda = \lambda_x = \lambda_z$ . A spontaneous increase of the width and a simultaneous decrease of the length marks the phase transformation to the  $L_{\alpha}$  phase. It is caused by the formation of planar micelles stacked along the  $z$  axis, and the corresponding oblate deformation of the coil that has to be accommodated in the hydrophobic layers. If no discontinuity of the volume occurs at the phase transformation, the discontinuities  $\Delta\lambda_x$  and  $\Delta\lambda_z$  are related by

$$(1 + \Delta\lambda_x)^2(1 - \Delta\lambda_z) = 1 \quad (4)$$

Notice that this behavior is just the opposite of what is found for hydrogels with a hexagonal phase, for which

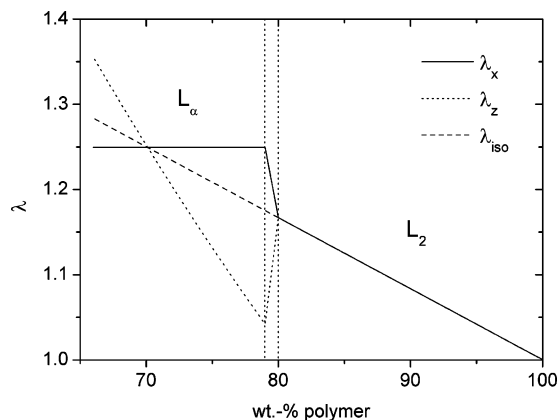


**Figure 6.** Schematic plot of the expected ideal hydroelastic behavior of a lamellar sample with the relative swelling coefficients parallel ( $\lambda_z$ ) and perpendicular ( $\lambda_x$ ) to the layer normal.

the length increases and the width decreases.<sup>8</sup> Upon further swelling with water in the supposedly ideal lamellar phase, that is on the left side of the phase transformation shown in Figure 6,  $\Delta\lambda_x$  will remain constant, but  $\Delta\lambda_z$  will continue to grow with a slope that is steeper than in the isotropic phase. Therefore,  $\lambda_x$  and  $\lambda_z$  will eventually cross each other at higher water concentration.

The results of the hydroelastic measurements on samples HG33*h* and HG65*h* are shown in Figures 7 and 8. For each sample three types of curves are shown: the relative swelling coefficients  $\lambda_x$  and  $\lambda_z$  (Figures 7a and 8a), the isotropic swelling coefficient  $\lambda_{iso} = (\lambda_z\lambda_x^2)^{1/3}$  (Figures 7b and 8b), and the reduced swelling coefficients  $\epsilon_x = \lambda_x/\lambda_{iso}$  and  $\epsilon_z = \lambda_z/\lambda_{iso}$  (Figures 7c and 8c).

For hydrogel HG33*h* the three regimes for the isotropic phase, the phase transformation, and the lamellar phase can be clearly recognized in Figure 7a. At the phase transformation, which has a certain width because of the coexistence of isotropic and lamellar phase, the hydrogel becomes shorter and broader, exactly as expected (cf. Figure 6). The micellar aggregation forces the polymer into a flattened, oblate conformation. Once the phase transformation is complete, the slopes of the curves change again. There are, however, some significant deviations from the predicted behavior. First, swelling in the  $L_2$  phase is not isotropic. Swelling with water has the same type of anisotropy, namely stronger swelling along  $x$ , as swelling with toluene (see above). Therefore, the same reason for this effect must be assumed, that is, a swelling anisotropy caused by the intrinsic network anisotropy due to stronger cross-linking between adjacent layers than within a single layer. Second, in the lamellar phase,  $\lambda_x$  does not remain constant but continues to grow. This indicates substantial swelling perpendicular to the layer normal, probably due to a defective porous lamellar structure, which is also evident from the diffusion studies. However, swelling is still stronger along  $z$  as expected, which is inferred from the steeper slope of  $\lambda_z$  compared to  $\lambda_x$ .

The volume degree of swelling  $q$ , calculated according to eq 2 from the experimental data of Figure 7a, serves as a check of the experimental accuracy. The cubic root of  $q$ , denoted by  $\lambda_{iso}$ , is a pseudo-isotropic swelling parameter describing the mere volume effect. In Figure 7b the calculated values of  $\lambda_{iso}$  are depicted as a function of the water concentration. The small differences in  $\lambda_{iso}$  observed upon repeated measurements shows that the

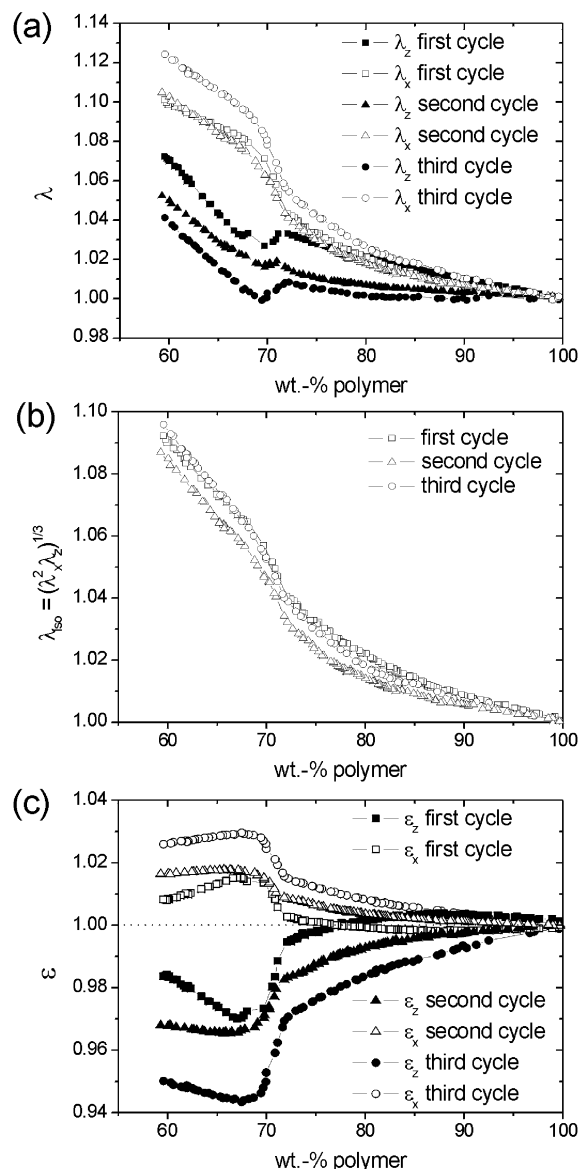


**Figure 7.** Hydroelastic results for HG33*h*: (a) swelling factors of the length ( $\lambda_z$ ) and the width ( $\lambda_x$ ) of the network; (b) isotropic swelling factor  $\lambda_{iso}$ ; (c) reduced swelling coefficients  $\epsilon_z$  and  $\epsilon_x$ . Three consecutive measurements (first to third cycle) are shown, each starting from the completely dried network.

volume stays almost the same for all cycles, which makes evident that the measurements are carried out correctly.

The slope of  $\lambda_{iso}$  as a function of the water concentration shows two discontinuities: one when reaching the two-phase region (coming from the isotropic  $L_2$  phase) and the other when reaching the pure lamellar phase. The concentrations at which these discontinuities are observed are in almost exact agreement with the phase diagram of the linear polymer, shown in Figure 1. The discontinuities of the slope, not taken into account in Figure 6, correspond to the discontinuity of the volume at the phase transformation and are consistent with a first-order transition. The change of slope within the isotropic phase furthermore shows that the partial molar volumes are not independent of concentration, a feature that can be explained by the specific interactions (hydrogen bonds) between the amphiphiles and water and is also not considered in Figure 6.

While Figure 7b illustrates the volume effect upon swelling with water, a plot of the reduced swelling

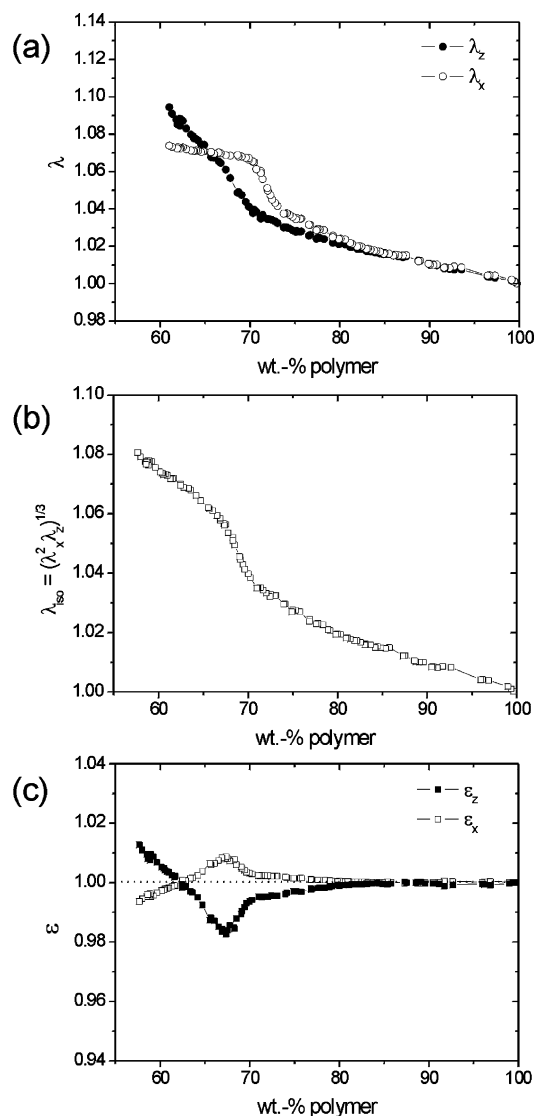


**Figure 8.** Hydroelastic results for HG65h: (a) swelling factors of the length ( $\lambda_z$ ) and the width ( $\lambda_x$ ) of the network; (b) isotropic swelling factor  $\lambda_{iso}$ ; (c) reduced swelling coefficients  $\epsilon_z$  and  $\epsilon_x$ .

coefficients  $\epsilon_x = \lambda_x/\lambda_{iso}$  and  $\epsilon_z = \lambda_z/\lambda_{iso}$ , as shown in Figure 7b makes the anisotropy of swelling evident. Plotting both  $\epsilon_x$  and  $\epsilon_z$  is redundant as uniaxiality requires that  $\epsilon_z = 1/\epsilon_x^2$ . Deviations of  $\epsilon$  from unity directly indicate an anisotropic deformation of the original network in the dry state. Thus, the curves in Figure 7c show the deviation from ideal isotropic swelling behavior and can therefore be related to an anisotropy of the chain deformation.

Comparing the different measurement cycles on the same sample an increase of anisotropy is observed, both in the isotropic and the lamellar phase. The disappearance of entanglements which are formed during the process of polymerization by repeated swelling and deswelling could provide a reasonable explanation of this effect. A similar behavior was observed in all samples.

The hydroelastic effect at the phase transformation is small compared to the corresponding thermoelastic effect observed in thermotropic nematics. For nematic side-chain liquid-crystal polymers an increase of their length up to 40% and more can be measured,<sup>42</sup> whereas the hydroelastic effect observed for the nonionic hydrogels of this study and other lamellar<sup>5</sup> or hexagonal<sup>8</sup>

lyotropic systems is just a few percent. One explanation for this difference may be the fact that two opposing effects contribute to the hydroelastic effect in lyotropics. On one hand, there is the change of the coil conformation caused by micellization. In lamellar systems this leads to a flattening of the coil and a shrinking parallel to the director ( $z$ ), while in hexagonal systems an elongation of the coil and a growth along the director is caused. In both cases, the second effect, due to the anisotropic swelling of the hydrophilic regions, is opposed to the first one. Swelling of a lamellar structure leads to an increase along the director, but swelling of a hexagonal phase leads to an increase perpendicular to it. As a result, the two contributions partly cancel each other and the remaining effect is small.

The hydrogel HG65h was synthesized at a different water concentrations as shown in Table 1. The precursor mixture has a higher amphiphile concentration than in sample HG33h. The lamellar phase exhibits its highest stability in this concentration range (cf. the phase diagram shown in Figure 1). We therefore expected a lamellar phase with less defects. The hydroelastic behavior of HG65h, shown again both in terms of the directly measured relative swelling coefficients  $\lambda_x$  and  $\lambda_y$  and in terms of the isotropic swelling coefficient  $\lambda_{iso}$  and the anisotropy  $\epsilon$ , is plotted in Figure 8. The characteristics of the swelling curves can be compared with HG33h. At the first glance, the shrinking along the  $z$  axis at the phase transformation is missing in Figure 8a. It is obviously completely compensated by the swelling along  $z$ . Figure 8c, however, reveals that the anisotropic behavior is essentially the same as that of HG33h. The behavior within the lamellar phase is noteworthy, since  $\lambda_x$  stays almost constant as theoretically expected for an ideal lamellar phase. This indicates that the lamellar structure is more perfectly ordered compared to HG33d, a result in agreement with the diffusion experiments discussed above. Also observed is the predicted crossing of  $\lambda_x$  and  $\lambda_z$ .

#### IV. Summary and Conclusion

Liquid single crystal hydrogels (LSCH) were synthesized via radical polymerization by incorporating an amphiphilic cross-linker molecule with reactive groups in both the hydrophobic and hydrophilic moieties directly into the lamellar liquid-crystalline phase of a rigid-rod-like amphiphile that is aligned by a magnetic field. Hydrogels with a macroscopically uniform director orientation were obtained that are stable against tensile forces in all three dimensions. Cross-linking within the liquid-crystalline phase results in an anisotropy of the network, which becomes evident by swelling experiments with a nonselective solvent in the isotropic phase.

The structure and ordering of these anisotropic hydrogels were investigated by a variety of methods on micro- and macroscopic length scales. The X-ray correlation length of about seven layers showed a rather low order on very small scales. The director orientation averaged over a mesoscopic scale of several micrometers, which was investigated by deuterium line shape analysis, was found to have a narrow distribution with its maximum parallel to the magnetic field and a full width at half-maximum of 13°. Diffusion NMR proved the existence of defects or pores in the lamellae on a similar length scale of several micrometers, but based on the absence of diffusion time-dependent diffusion coefficients gave also an estimation of the minimal extension

of homogeneous domains of the order of 10  $\mu\text{m}$  (parallel to the director) by 30  $\mu\text{m}$  (perpendicular to the director).

The temperature-dependent obstruction factors for diffusion parallel to the layer normal showed a characteristic step at around 312–314 K. Whether this is caused by inherent stresses due to an anisotropic thermal change of dimensions of the elastomer or whether it is triggered by a temperature-induced change of the lyotropic phase structure analogous to an  $L_\alpha$ – $L_3$  transformation remains to be further investigated.

The macroscopic thermodynamic behavior evident from swelling experiments is consistent with established network theories. The direct comparison of the hygroelastic response with the thermoelastic correspondent of thermotropic liquid-crystalline elastomers shows a similar direct mechanical effect at the formation of the liquid-crystalline phase. However, the hygroelastic effect, which reflects the coupling between liquid-crystalline phase structure and the network chain conformation, is much weaker than its thermoelastic analogon. The reason for this behavior is still unknown. Obviously the formation of ordered, nonionic, micellar aggregates does not require considerable rearrangement of the network strands. Here it must be noted that very recent results on ionic systems reveal a much stronger hygroelastic response, which can be explained by an increased Kuhn length of the main-chain segments due to the ionic charges.

The comparison of two different hydrogels that were synthesized with a different content of water showed that ordering and structure are much better in the system with the lower content of water whose composition is close to the one with maximum temperature of the lamellar phase. Consistent results pointing out the difference in order were obtained by such different methods as diffusion NMR and hygroelastic measurements.

Future investigations should include the design of new types of amphiphiles which allow an end-on architecture of the polysoaps instead of the side-on architecture presented here. The latter is expected to disturb the order of the amphiphiles, and better ordered phases are expected for polysoaps with end-on attached amphiphilic chains. This should also help to understand if and how the type of attachment influences the coupling between liquid-crystalline phase and polymer network.

**Acknowledgment.** The authors are greatly indebted to the Deutsche Forschungsgemeinschaft (Sonderforschungsbereich 428) and the Fonds der Chemischen Industrie for financial support. They thank Laura Hartmann for her help with the dye diffusion experiments.

## References and Notes

- (1) de Gennes, P. G. *C. R. Scéances Acad. Sci., Ser. B* **1975**, *281*, 101.
- (2) Finkelmann, H.; Kock, H. J.; Rehage, G. *Makromol. Chem., Rapid Commun.* **1981**, *2*, 317.
- (3) Amigó-Melchior, A.; Finkelmann, H. *Polym. Adv. Technol.* **2002**, *13*, 363.
- (4) Bauer, H.; Hermes, R. *Pharmazie* **1995**, *50*, 481.
- (5) Fischer, P.; Finkelmann, H. *Prog. Colloid Polym. Sci.* **1998**, *111*, 127.
- (6) Fischer, P.; Schmidt, C.; Finkelmann, H. *Macromol. Rapid Commun.* **1995**, *16*, 435.
- (7) Löffler, R.; Finkelmann, H. *Makromol. Chem., Rapid Commun.* **1990**, *11*, 321.
- (8) Weiss, F.; Finkelmann, H. *Macromolecules* **2004**, *37*, 6587.
- (9) Keller-Griffith, R.; Ringsdorf, H.; Vierengel, A. *Colloid Polym. Sci.* **1986**, *264*, 924.
- (10) Ringsdorf, H.; Schlarb, B.; Venzmer, J. *Angew. Chem.* **1988**, *100*, 117.
- (11) Lindner, N.; Köbel, M.; Sauer, C.; Diele, S.; Jokiranta, J.; Tschierske, C. *J. Phys. Chem. B* **1998**, *102*, 5261.
- (12) Lühmann, B.; Finkelmann, H. *Colloid Polym. Sci.* **1987**, *265*, 506.
- (13) Schafheutle, M. A.; Finkelmann, H. *Liq. Cryst.* **1988**, *3*, 1369.
- (14) Lee, M.; Cho, B.-K.; Kim, H.; Zin, W.-C. *Angew. Chem.* **1998**, *110*, 661.
- (15) Amigó-Melchior, A.; Finkelmann, H. *Colloid Polym. Sci.* **2002**, *280*, 207.
- (16) Schafheutle, M. A.; Finkelmann, H. *Liq. Cryst.* **1988**, *3*, 1369.
- (17) Brodowsky, H. M.; Boehnke, U.-C.; Kremer, F. *Langmuir* **1999**, *15*, 274.
- (18) Stannarius, R.; Köhler, R.; Dietrich, U.; Lösche, M.; Tolksdorf, C.; Zentel, R. *Phys. Rev. E* **2002**, *65*, 041707.
- (19) Schüring, H.; Stannarius, R.; Tolksdorf, C.; Zentel, R. *Macromolecules* **2001**, *34*, 3962.
- (20) Gebhard, E.; Zentel, R. *Macromol. Chem. Phys.* **2000**, *201*, 902.
- (21) Brodowsky, H. M.; Kremer, F.; Gebhard, E.; Zentel, R. *Ferroelectrics* **2000**, *243*, 115.
- (22) Mitsunobu, O. *Synthesis* **1981**, 1.
- (23) Stejskal, E. *J. Chem. Phys.* **1965**, *43*, 3597.
- (24) Stejskal, E.; Tanner, J. *J. Chem. Phys.* **1965**, *42*, 288.
- (25) Callaghan, P. T. *Principles of Nuclear Magnetic Resonance Microscopy*; Clarendon Press: New York, 1993.
- (26) Mills, R. *J. Phys. Chem.* **1973**, *77*, 685.
- (27) Assfalg, N.; Finkelmann, H. *Macromol. Chem. Phys.* **2001**, *202*, 794.
- (28) Friedel, G.; Grandjean, F. *Bull. Soc. Fr. Mineral.* **1910**, *33*, 409.
- (29) Gray, G. W.; Goodby, J. W. *Smectic Liquid Crystals*; Leonard Hill: Glasgow, 1984.
- (30) Benton, W. J.; Fort, T. J.; Miller, C. A. *53rd Ann. Fall Technol. Conf. and Exh. of Soc. Pet. Eng. of AIME*, Houston TX, 1978.
- (31) Benton, W. J.; Miller, C. A. *Prog. Colloid Polym. Sci.* **1983**, *68*, 71.
- (32) Lovell, R.; Mitchell, G. R. *Acta Crystallogr. A* **1981**, *37*, 135.
- (33) Mitchell, G.; Windle, A. *Developments in Crystalline Polymers*; Basset, D., Eds.; Elsevier: London, 1984; p 140.
- (34) Adhikari, B.; Vora, R. A.; Paul, R. *Mol. Cryst. Liq. Cryst.* **1996**, *287*, 129.
- (35) Honerkamp, J.; Weese, J. *Continuum Mech. Thermodyn.* **1990**, *2*, 17.
- (36) Weese, J. *Comput. Phys. Commun.* **1992**, *69*, 99.
- (37) Winterhalter, J.; Maier, D.; Grabowski, D. A.; Honerkamp, J.; Müller, S.; Schmidt, C. *J. Chem. Phys.* **1999**, *8*, 4035.
- (38) Gaemers, S.; Bax, A. *J. Am. Chem. Soc.* **2001**, *123*, 12343.
- (39) Callaghan, P. T. *Aust. J. Phys.* **1984**, *37*, 359.
- (40) Kleinschmidt, F. Dissertation, University Freiburg, 2005.
- (41) Porte, G.; Appell, J.; Bassereau, P.; Marignan, J. *J. Phys. (Paris)* **1989**, *50*, 1335.
- (42) Küpfer, J.; Finkelmann, H. *Makromol. Chem., Rapid Commun.* **1991**, *12*, 717.

MA0514790